Broad-Band High-Power Amplifier Using Spatial Power-Combining Technique

Pengcheng Jia, *Member, IEEE*, Lee-Yin Chen, *Student Member, IEEE*, Angelos Alexanian, *Member, IEEE*, and Robert A. York, *Senior Member, IEEE*

***Abstract*—High power, broad bandwidth, high linearity, and low noise are among the most important features in amplifier design. The broad-band spatial power-combining technique addresses all these issues by combining the output power of a large quantity of microwave monolithic integrated circuit (MMIC) amplifiers in a broad-band coaxial waveguide environment, while maintaining good linearity and improving phase noise of the MMIC amplifiers. A coaxial waveguide was used as the host of the combining circuits for broader bandwidth and better uniformity by equally distributing the input power to each element. A new compact coaxial combiner with much smaller size is investigated. Broad-band slotline to microstrip-line transition is integrated for better compatibility with commercial MMIC amplifiers. Thermal simulations are performed and an improved thermal management scheme over previous designs is employed to improve the heat sinking in high-power application. A high-power amplifier using the compact combiner design is built and demonstrated to have a bandwidth from 6 to 17 GHz with 44-W maximum output power. Linearity measurement has shown a high third-order intercept point of 52 dBm. Analysis shows the amplifier has the ability to extend spurious-free dynamic range by $N^{2/3}$ times. The amplifier also has shown a residual phase floor close to −140 dBc at 10-kHz offset from the carrier with 5–6-dB reductions compared to a single MMIC amplifier it integrates.**

***Index Terms*—Broad-band, coaxial waveguide, finline, high power, power combiner, spatial.**

I. Introduction

INVENTED in the 1940s, the traveling-wave tube amplifier (TWTA) has become a key element in microwave systems for radar, satellite communication, and wireless communication. An alternative to the TWTA is a power combiner. The corporate combining technique will lead to very high combining loss when integrating a large amount of amplifiers, while the spatial power-combining technique was proposed with the goal to combine a large quantity of solid-state amplifiers efficiently and improve the output power level to be competitive with TWTAs. The University of California at Santa Barbara's (UCSB) Microwave Group attempted a "tray" scheme inside a waveguide to achieve broad bandwidth, better thermal management, and more efficient power collection [1]–[3]. Employing the "tray" scheme, we demonstrated an X-band power amplifier with 120-W output power using an oversized WR-94 rectangular waveguide.

However, the bandwidth of the rectangular waveguide is limited. In addition, the dominant TE_{10} mode inside the rectangular waveguide leads to nonuniform illumination of the loaded antenna trays inside the waveguide. Hence, the output power experiences a soft saturation that will deteriorate the linearity or lead to larger backoff in output power to satisfy the requirement of linearity. To broaden the bandwidth and to meet the requirement of linearity, we extend the "tray" approach from the rectangular waveguide to coaxial waveguide. A multioctave bandwidth amplifier achieved bandwidth from 3.5 to 14 GHz with good linearity using an oversized coaxial waveguide combiner [4].

The design of a compact broad-band passive combiner was elaborated upon in [5]. A significant reduction in size has been achieved while maintaining a 6–18-GHz bandwidth and capacity for 32 microwave monolithic integrated circuit (MMIC) amplifiers. A broad-band slotline to microstrip-line transition was developed and monolithically integrated with the slotline antennas to eliminate a troublesome bond-wire transition in earlier design and provide better compatibility with commercial MMIC amplifiers. The spectral-domain method (SDM) is applied to compute the field in the structure, and small reflection theory is applied again to synthesize the waveguide taper and optimize the finline taper array. The high-power amplifier system was first introduced in [6]. In this paper, we report on the details of the high-power amplifier using the compact coaxial waveguide combiner design, which has shown 6–17-GHz bandwidth with 44-W maximum output power along with good linearity and high dynamic range. That makes it a good rival for current dominant traveling-wave tube (TWT) amplifiers.

For the sake of abbreviation, we use the term "combiner" in this paper to refer to the amplifier using the compact broad-band combiner structure.

II. Assembly and Thermal Analysis

In power amplifiers, the heat generated by the MMIC amplifiers needs to be effectively dissipated to the ambient envi-

Manuscript received April 15, 2003. This work was supported by the Office of Naval Research (ONR) Multiuniversity Research Initiative (MURI) IMPACT program under Grant N00014-96-1-1215, by the ONR CANE MURI Program, and by the Army Research Office MURI Program under Grant DAAG55-98-1-0001.

P. Jia was with the Electrical Engineering Department, University of California at Santa Barbara, Santa Barbara, CA 91320 USA. He is now with CAP Wireless Inc., Newbury Park, CA 91320 USA (e-mail: jiapc@capwireless.com).

L.-Y. Chen was with the Electrical Engineering Department, University of California at Santa Barbara, Santa Barbara, CA 91320 USA. She is now with Agile Materials and Technologies, Goleta, CA 93117 USA.

A. Alexanian is with Narad Networks, Westford, MA 01886 USA.

R. A. York is with the Electrical Engineering Department, University of California at Santa Barbara, Santa Barbara, CA 91320 USA.

Digital Object Identifier 10.1109/TMTT.2003.819766

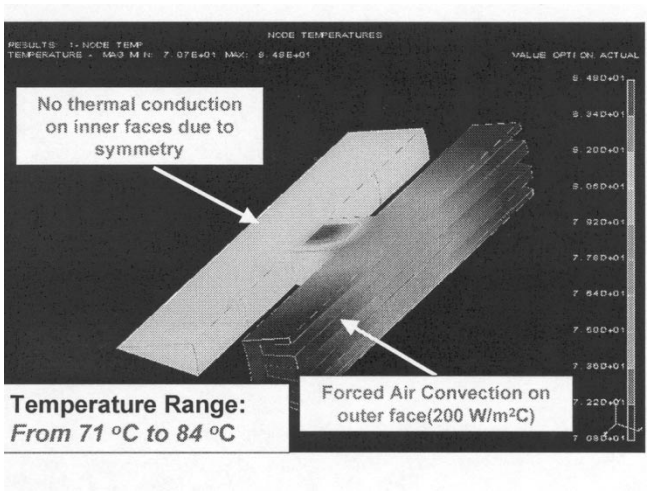

Fig. 1. Thermal simulation of the metal tray.

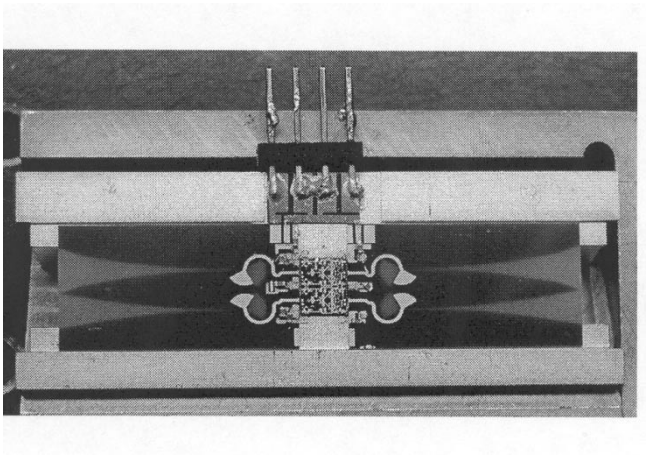

Fig. 2. One of the circuit trays in the combiner.

ronment. Heat transfer occurs as a result of the temperature gradient between the MMIC amplifiers and the environment. The heat is dissipated into the air by two modes: conduction and convection.

Heat is conducted by the metal tray to its outside surface first. Since copper is only inferior to silver in thermal conductivity at room temperature and is 1.6× better than aluminum, we chose copper as the material at the price of higher weight and cost. MMIC amplifiers were directly attached to the copper–molybdenum (Cu/Mo) subcarriers to avoid thermal expansion mismatch problems. To minimize thermal resistance, two different eutectic solders, Au/Sn and Au/Ge, which have different melting points, were used to solder the MMIC to the Cu/Mo subcarrier and Cu/Mo subcarrier to the metal tray, respectively.

The ambient environment absorbs the heat from the carriers by convection. Fans were used to accelerate the heat-transfer process.

The irregular configuration makes the heat transfer of the structure difficult to be calculated analytically. As a result, a mechanical software package, SDRC's I-deas 8.0, was chosen to simulate the heat transfer. In the thermal model, we only simulated 1/16th of the waveguide structure due to the symmetry. Since all the MMIC amplifiers generate the same amount of heat, there is no heat transfer between metal trays. Thus, it is safe to assume an insulation layer on the interface between trays. The heat is conducted to the outside surface and convectively dissipated into the air. The Cu/Mo subcarrier and eutectic solder layers are all included in the thermal model.

The wedge-shaped tray has a limited surface area due to its small radius. To help dissipate heat, fins were machined into the outside surface to increase the surface area. During operation, the worst case is that no RF input power is applied and 100% of the dc power is dissipated. In the thermal simulation, a heat source of 20 W is applied to the surface of the Cu/Mo subcarrier. Fig. 1 shows that the tray temperature is mostly in the 70 °C range, with 84 °C at the hottest spot when a thermal convection coefficient of 200 $\mathrm{W/m^2}$ C is applied on the outside surface. This temperature can be reduced by increasing the surface area or increasing the thermal convention coefficient.

The assembled circuit tray is shown in Fig. 2. The two-channel MMIC amplifier sits on the bridge that connects the inner and outer sections. Input and output antennas were epoxyed on both sides with bonding wires connected to the MMIC amplifier. Bias pins were epoxyed at the outer side of the tray. DC currents are input to MMIC amplifiers through biasing lines and bonding wires. The overall dc impedance from pins to the MMIC amplifier's pads is from 0.2 to 0.3 Ω.

III. Small-Signal Measurements

As explained in [5], the performance of the waveguide structure and finline transition is simulated by *HFSS*, a three-dimensional (3-D) finite-element method (FEM) simulator. We exported the S-parameter results from *HFSS* to S2p files, and then imported them into the Agilent *Advance Design System* (*ADS*).

The combiner integrates 32 channels of MMIC power amplifiers. Due to the symmetric field distribution, as analyzed in [4], we divided the combiner into 32 parallel identical sections from the input to output ends and simulated only one of 32 channels in the *ADS* model. As shown in [6], the circuit model included the input/output waveguide tapers, finline transitions, a lossy matching network, and a MMIC amplifier. The one-section simulation represents the overall amplifier because the spatial power-combining theory has proven that the power is evenly distributed to and combined from each channel and the overall gain is the same as one channel.

The TGA9092 MMIC amplifier has a gain in excess of 25 dB, which very easily causes oscillation problems inside a waveguide environment when the output to input isolation is only slightly higher than 20 dB at the lowest points. The circuit becomes stable when the overall gain is reduced within 20 dB after the insertion of a lossy matching network. The results from both the measurement and simulation are shown in Fig. 3. Agreement between measurement and ADS simulation verifies the effectiveness of the modeling. There is around 8-dB difference in the gain between the MMIC amplifier and combiner, which is caused by the lossy matching network.

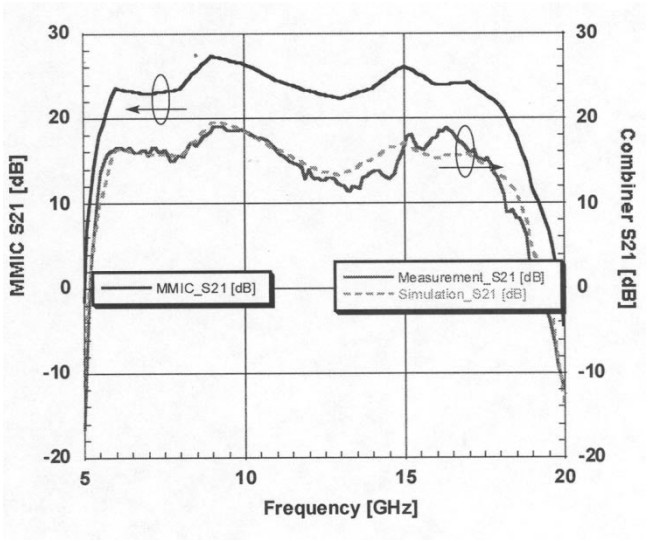

Fig. 3. Comparison of simulation and measurement of the combiner and MMIC amplifier.

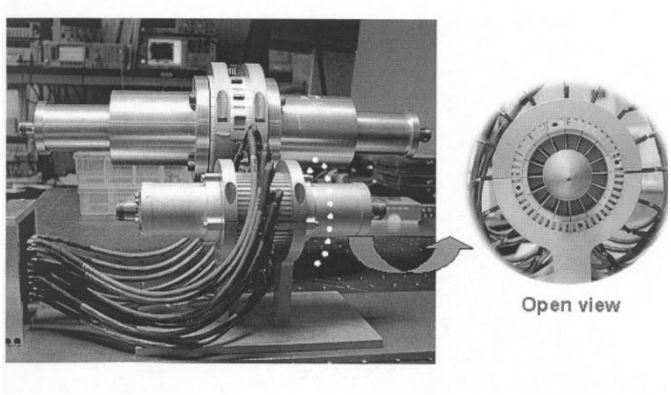

Fig. 4. Compact combiner compared with the previous design and its open view.

IV. Power Measurements

Fig. 4 shows the assembly of the combiner system. The bias lines were connected from a biasing board to the 16 individual circuit trays. The KEPCO eight-channel power supply and an Agilent power supply were connected to a biasing board, which provides both drain currents and gate voltages.

The input power level was chosen to be 30 dBm. A frequency sweep measurement result is shown in Fig. 5. A maximum power of 44 W is obtained at 10 GHz. The gain curve followed a similar shape to the small-signal gain curve in Fig. 3, with the exception that gain compression occurs differently over the band. The 3-dB bandwidth is from 6 to 17 GHz. We noted that two MMIC amplifiers of the 32-MMIC combiner were nonfunctional in the process of the power measurement. The small-signal gain of the combiner is reduced to 18.2 dB, which is approximately 0.4 dB smaller than the small-signal gain of the combiner when all MMIC amplifiers are functional. The combiner's output power was measured with 30 working MMIC amplifiers. It is 88% of the 32-MMIC combiner's output power basing on the graceful degradation theory [7]. This degradation also leads to the reduction in power-combining efficiency.

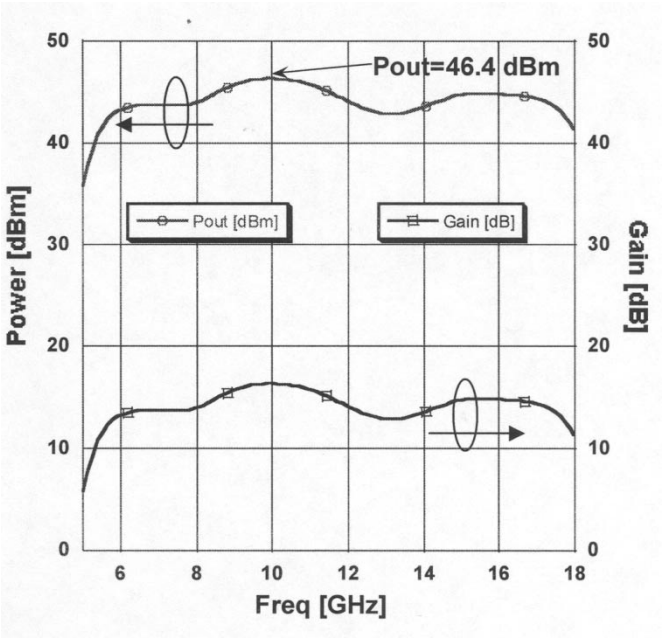

Fig. 5. Frequency sweep at 30-dBm input power.

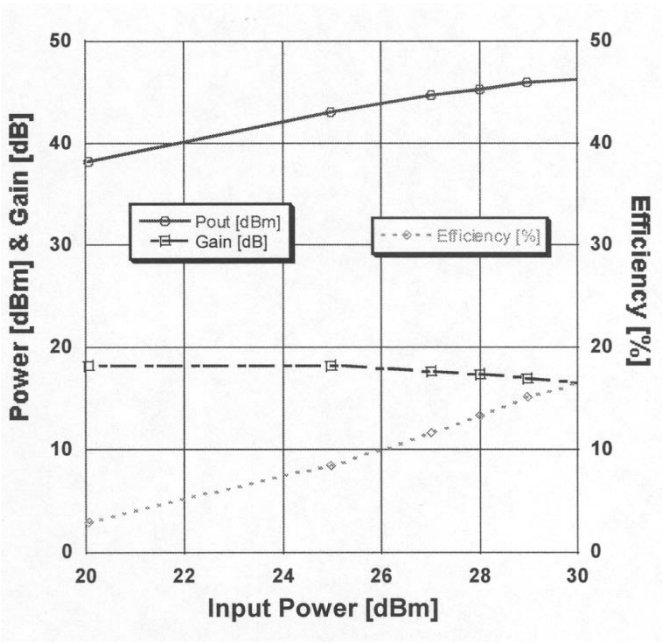

Fig. 6. Power sweep at 10 GHz.

The power-added efficiency (PAE), output power, and gain were swept over the input power at 10 GHz, as shown in Fig. 6. At 30-dBm input power, the gain is compressed by 1.8 dB. The PAE was approximately 17% at an output power of 44 W.

To evaluate the change of the third-order intercept point (IP3) point in power combining, we compared the third-order intermodulation component (IM3) of a MMIC amplifier and the combiner. For a MMIC amplifier, the fundamental and IM3 output power is expressed as

$$P_{\text{out}} = G_m P_{\text{in}}$$
$$\text{IM}_3 = A P_{\text{in}}{}^3 \tag{1}$$

where G_m is the gain of the MMIC amplifier, and A is the coefficient for IM_3.

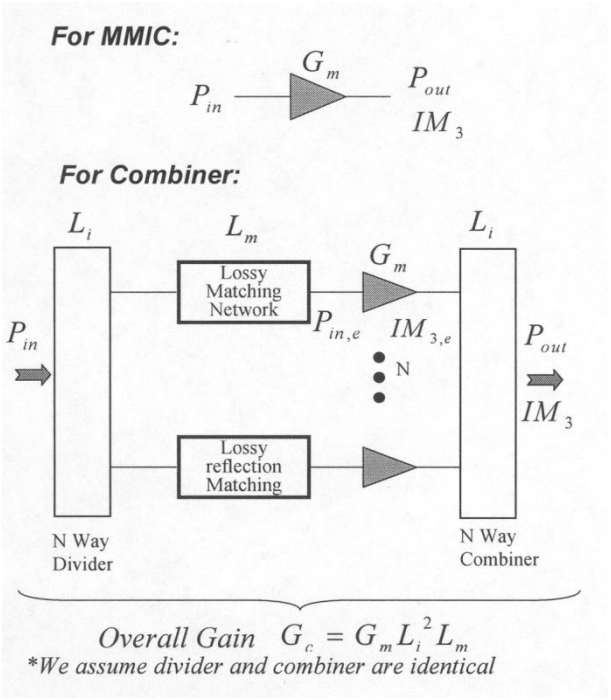

Fig. 7. Linearity analysis for the MMIC amplifier and combiner.

The comparison of IM3 between a single MMIC and the combiner is shown in Fig. 7. The output IP3 (OIP3) is the output power at the IP3 point, where the linearly extrapolated fundamental output power $P_{\rm out} = {\rm IM}_3$. The OIP3 of a MMIC amplifier is

$$\mathrm{OIP3}_m = \left(\frac{{G_m}^3}{A}\right)^{\frac{1}{2}}. \tag{2}$$

For a combiner, we have

$$\begin{aligned} G_c &= G_m {L_i}^2 L_m, \\ P_{\rm out} &= G_c P_{\rm in} = G_m {L_i}^2 L_m P_{\rm in} \end{aligned} \tag{3}$$

where L_m is the loss of the lossy matching network and we assume the passive N-way divider and combiner are identical.

For each MMIC amplifier in the combiner, we have

$$\begin{aligned} P_{{\rm in},e} &= \frac{P_{\rm in} L_i L_m}{N} \\ {\rm IM}_{3,e} &= A {P_{{\rm in},e}}^3 \end{aligned} \tag{4}$$

where N is the number of channels in the combiner.

${\rm IM}_{3,e}$ from each MMIC amplifier are added in the same way as the fundamental signal. The sum of ${\rm IM}_{3,e}$ at the output port is expressed in ${\rm IM}_3$ as

$${\rm IM}_3 = N{\rm IM}_{3,e} L_i = NA {P_{{\rm in},e}}^3 L_i. \tag{5}$$

We then have

$$\begin{aligned} P_{\rm out} &= {\rm IM}_3 \\ &= NA \left(\frac{P_{\rm in} L_i L_m}{N}\right)^3 L_i \\ \mathrm{OIP3}_c &= N L_i \left(\frac{{G_m}^3}{A}\right)^{\frac{1}{2}} \end{aligned} \tag{6}$$

where $\mathrm{OIP3}_c$ is the OIP3 of the combiner.

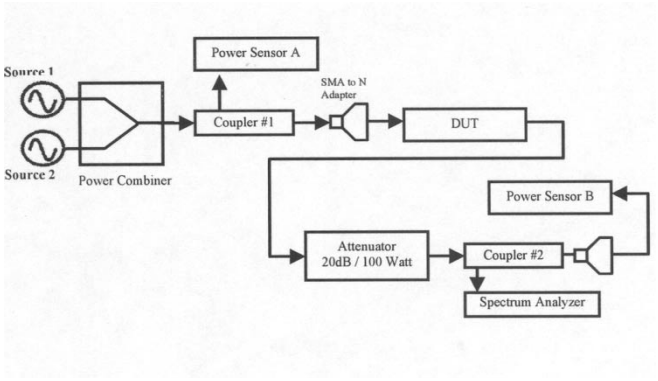

Fig. 8. Intermodulation distortion measurement setup.

Comparing (2) and (6), we conclude that

$$\mathrm{OIP3}_c = N L_i \mathrm{OIP3}_m. \tag{7}$$

For a 32-channel combiner with L_i of 1 dB, the combiner will have a factor of 14-dB improvements in the OIP3 over a MMIC amplifier. We note that the OIP3 has no relationship with the lossy matching network. The same improvement will be observed when we use the lossy matching network. The relationship between the fundamental component and third-order component also remains the same for the combiner and MMIC amplifier.

The intermodulation distortion was measured by two tones at 10 GHz with a separation of 1 MHz in spectrum. The measurement setup is shown in Fig. 8. The system's losses from the couplers, connectors, adaptors, and cables were calibrated first. After the device-under-test (DUT) was added in the measurement setup, the fundamental and IM3s were read from the spectrum analyzer and were then corrected with the calibration data.

The IMD measurement result of the combiner with 30 working MMIC amplifiers is shown in Fig. 9. The small change of the IM3 curve shape is due to the unequally driving of the MMIC amplifiers because of the nonfunctioning of two MMIC amplifiers. The MMIC amplifiers adjacent to the broken MMIC amplifiers saturate in amplitude faster when the input signal increases. However, since the IP3 point is determined by the linear part of the fundamental and IM3 traces, it will not be changed in this case.

At 10 GHz, the OIP3 is 52 dBm compared to around 38 dBm of a single MMIC, which is very close to a 14-dB improvement over a single MMIC amplifier, as indicated by (7).

V. Spurious-Free Dynamic Range (SFDR)

Many communication systems, such as those transponding multiple carriers with code-division multiple-access (CDMA) technology, requires a high SFDR. The SFDR represents the ability of a system to detect or boost input signals in the presence of noise and other strong signals. It is determined by the system's noise figure and intermodulation point. The initial description of SFDR in a spatial combiner system is presented in [8], but the authors concluded an N-times improvement in the SFDR for the combiner over composed MMIC amplifiers. Here, we will give a more accurate and detailed analysis.

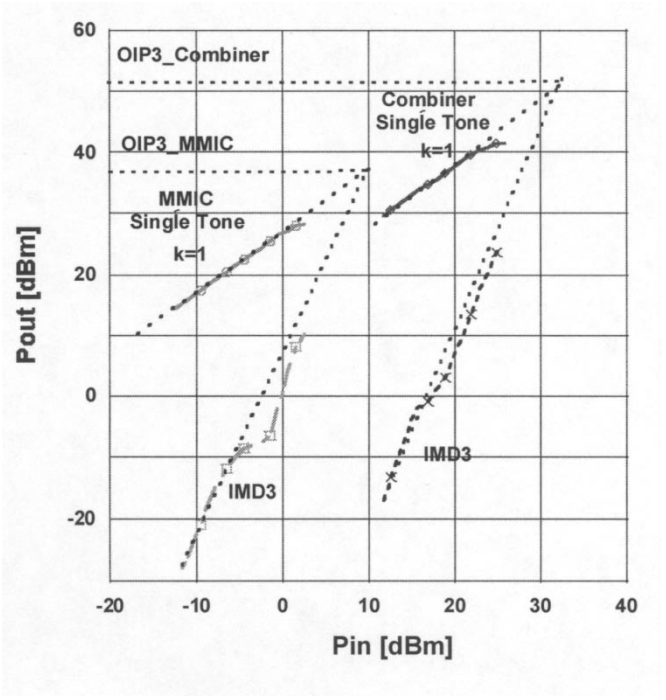

Fig. 9. Comparison of IMD3 between the MMIC amplifier and combiner.

The SFDR ranges from the receiver's noise floor to an upper limit often defined as the power when an IM3 tone (for two equal input tones) equals to the receiver's noise floor power. This yields the expression

$$\mathrm{SFDR} = \left(\frac{\mathrm{OIP3}}{FGk_BT_0\Delta f}\right)^{\frac{2}{3}} \tag{8}$$

where F is the receiver noise factor, G is the gain, Δf is the instantaneous bandwidth, k_B is Boltzman's constant, and T_0 is the ambient temperature.

From the expressions, the scaling behavior of the SFDR in an amplifier is obvious. For a combiner system, the gain G and noise figure F do not scale, only OIP3 scales with the factor of N. The SFDR is proportional to $N^{2/3}$. This is shown in

$$\begin{aligned} G_c &= G_m {L_i}^2 L_m \\ F_c &\approx F_m {L_i}^{-1} {L_m}^{-1} \\ \mathrm{OIP3}_c &= NL_i\mathrm{OIP3}_m \\ \mathrm{SFDR}_c &= N^{\frac{2}{3}}\mathrm{SFDR}_m. \end{aligned} \tag{9}$$

where subscript c refers to the combiner, m refers to the MMIC amplifier, L_i is the loss of the input/output combining circuitry, and L_m is the loss of the lossy matching network.

From (9), we can deduct that the combiner has a 10-dB improvement in the SFDR over a single MMIC amplifier.

VI. Residual Phase Noise

Residual phase noise is the added noise to input signal's phase when the signal is processed by a two-port device. It is commonly used to evaluate the deterioration of a signal's phase noise after it passes a two-port device.

If we assume small noise fluctuation in each channel, the output noise of the combiner in terms of input noise and individual amplifier noise contributions is

$$\begin{aligned} B_{\mathrm{out}} &= \frac{1}{\sqrt{N}}\sum_{i=1}^{N} b_{\mathrm{out},i} \\ &= \frac{AG}{N}\sum_{i=1}^{N}\cos(\omega t + \delta\theta_{\mathrm{in}} + \delta\varphi_i) \\ &= \frac{AG}{N}\left\{N\cos(\omega t) - \left[\sum_{i=1}^{N}(\delta\theta_{\mathrm{in}} + \delta\varphi_i)\right]\sin(\omega t)\right\} \\ &= AG\cos(\omega t + \delta\theta_{\mathrm{out}}) \end{aligned} \tag{10}$$

where $\delta\theta_{\mathrm{out}} = \delta\theta_{\mathrm{in}} + 1/N\sum_{i=1}^{N}\delta\varphi_i$ [9].

Added noise from each amplifier is $\langle|\delta\bar{\varphi}|^2\rangle$, making the output noise

$$\left\langle|\delta\tilde{\theta}_{\mathrm{out}}|^2\right\rangle = \left\langle|\delta\tilde{\theta}_{\mathrm{in}}|^2\right\rangle + \frac{1}{N}\left\langle|\delta\tilde{\varphi}|^2\right\rangle. \tag{11}$$

The second part in (11) is the residual phase noise. It will be improved by a factor of N if all the added noise is uncorrelated. If the input phase noise is small compared to the residual phase noise, we will also see approximately an N-times reduction in the overall output phase noise.

The residual phase noise is measured with an HP3048 phase-noise system. As shown in Fig. 10, the input signal is divided into two identical channels by a power divider. The phases of the two channels are adjusted into quadrature by a phase shifter. An attenuator is added to adjust the input power at the L and R port of HP11848 at the proper level. The HP11848 phase-noise interface has a double balanced mixer as the phase detector. HP11848 demodulates the RF signal to baseband noise signal and the baseband signal's spectrum is computed by the HP3561A dynamic signal analyzer. If the peak phase deviation is smaller than 0.2 rad, the RF signal phase-noise spectrum is one-half of the baseband noise spectrum.

The residual phase-noise measurement results of the high-power-combiner system and its composed MMIC amplifier are shown in Fig. 11. We observed spikes in this figure, which are the spurs from the dc-bias lines. The residual phase-noise floor is close to -140 dBc at a 10-kHz offset from the carrier frequency. However, instead of N times, which is corresponding to 15 dB, only 5–6-dB residual phase-noise reduction is observed from the phase-noise spectrum.

The residual noise of a 1-W medium power-combiner system [4] and its composed MMIC amplifier are then measured for comparison, and the result is shown in Fig. 12. An approximate average of 15-dB improvements in residual phase noise is observed. The residual phase noise is lower than -150 dBc at a 10-kHz offset from the carrier frequency. The very low residual phase-noise level is because of the phase-noise reduction from the combiner system and that the MMIC used in this combiner system is designed for low-noise applications. The residual phase-noise spectrum of the medium power combiner follows a 10-dB/decade curve from 1-Hz to 1-kHz offset from carrier frequency, which is the characteristic of $1/f$ noise. In the low-noise MMIC amplifier we used for the medium

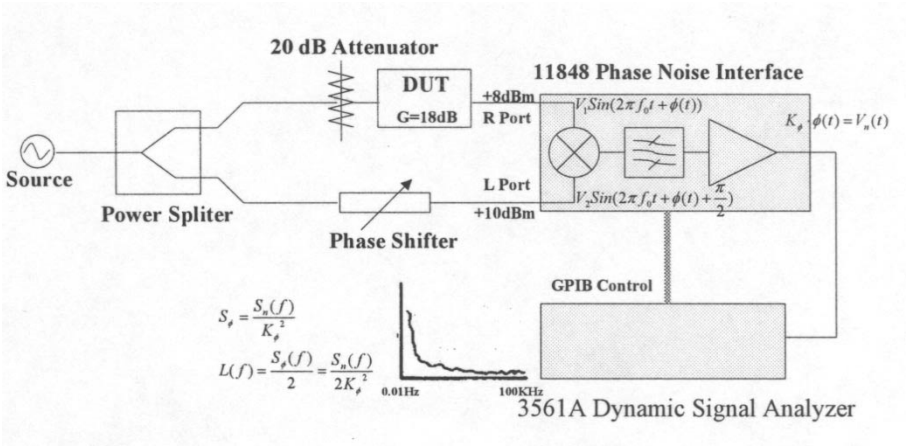

Fig. 10. Residual phase-noise measurement setup.

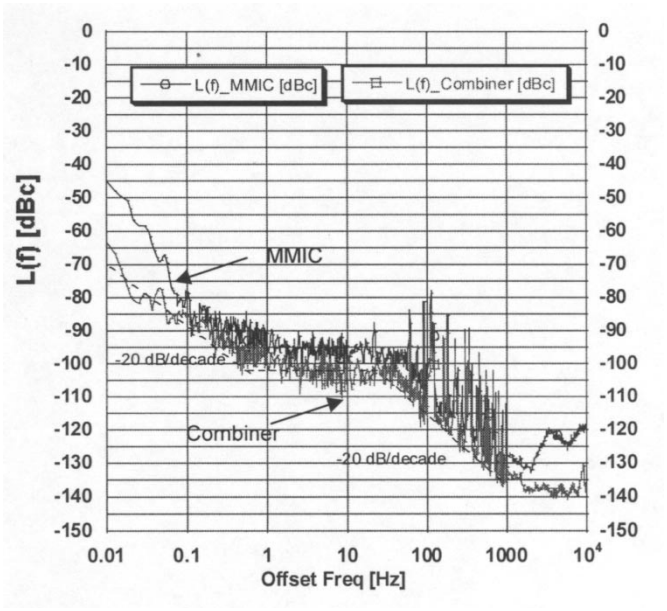

Fig. 11. Residual phase-noise measurement of the high-power combiner and its composed MMIC amplifier.

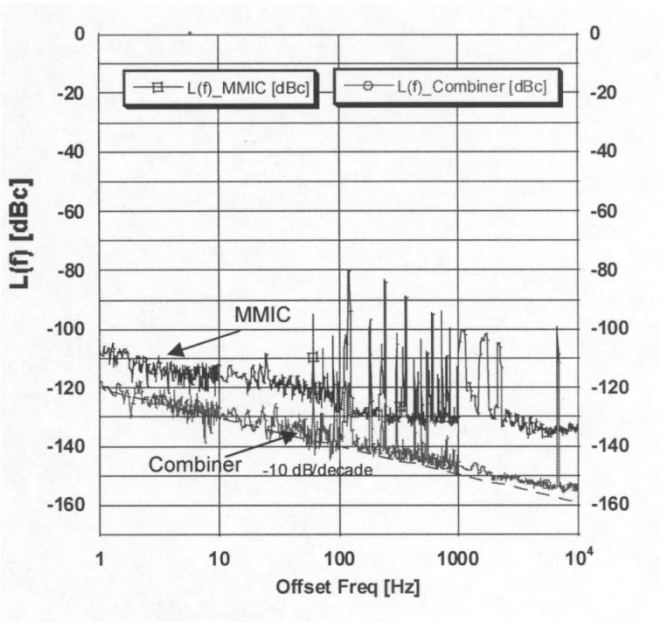

Fig. 12. Residual phase-noise measurement of the 1-W medium power combiner and its composed MMIC amplifier.

power-combiner system, $1/f$ noise is the dominant source of phase noise. The $1/f$ noise is from the imperfect material of each GaAs device and is uncorrelated for each MMIC amplifier. From (11), 15-dB reductions in residue phase noise are expected, which agrees well with the measurement results.

The reason for the smaller reduction in residual phase noise in the high-power-combiner system is the partial correlation of the phase-noise sources in each channel of the combiner. The residual phase noise come from either the direct additive noise to the RF band or the multiplicative noise, which is transferred from baseband to the RF band due to the nonlinearity of the active devices. In the combiner, the multiplicative noise on the bias lines is upconverted into the sideband of the carrier due to the nonlinearity of the amplifiers. Since the current is very high, the multiplicative bias line noise is dominant in all of the phase-noise sources. Since the 32 MMIC amplifiers are driven by one KEPCO eight-channel dc power supply, multiplicative noise in each MMIC amplifier is partially correlated. Every four MMIC amplifiers have the same bias line noise by sharing the same power apply channel and there are also correlations between different dc supply channels in the KEPCO power supply because of the common ground line. We did not observe a $1/f$ curve from 1-Hz to 1-kHz offset from carrier frequency for the reason that the $1/f$ noise is inferior compared with the dc line noise. Instead, a low-pass characteristic curve is observed in the phase-noise spectrum. That is because the capacitors used in the dc-bias line forms low-pass filters and the low-pass filtered multiplicative noise spectrum is transferred to the sideband of the RF carrier.

If we integrate a voltage regulator for each MMIC amplifier, asides from adding a voltage protection feature to each MMIC amplifier, we will decorrelate the bias line noise. We will then be able to achieve the same phase-noise reduction as the medium power amplifier does.

VII. Conclusion

A compact coaxial waveguide combiner structure has been presented in this paper. The total size of the new system is reduced dramatically compared to previous ones. In addition, with the monolithic integration of the slotline-to-microstrip transition, fabrication of the system becomes easier with better performance. The amplifier using the compact coaxial waveguide combiner shows the 3-dB bandwidth from 6 to 17 GHz with a maximum power of 44 W. We maintain the combiner's linearity similar to that of a MMIC amplifier, while improving the OIP3 of the combiner to 52 dBm, which is 14 dB higher than that of a single MMIC amplifier used in the combiner. The combiner system also shows the ability to extend SFDR and lower the residual phase-noise floor. These features makes this amplifier a good candidate for high-power amplifiers in wireless and satellite communication base-stations.

Acknowledgment

The authors wish to acknowledge the assistance of Dr. P. F. Maccarini, University of California at Santa Barbar (UCSB). The authors also want to thank the Structural Dynamics Research Corporation (SDRC), now the Electronic Data Systems Corporation (EDS), Planto, TX, for supplying the I-deas simulator under their Consortium Program.

References

[1] A. Alexanian and R. A. York, "Broadband waveguide-based spatial combiner," in *IEEE MTT-S Int. Microwave Symp. Dig.*, vol. 3, Denver, CO, June 8–13, 1997, pp. 1139–1142.

[2] N.-S. Cheng *et al.*, "40-W CW broad-band spatial power combiner using dense finline arrays," *IEEE Trans. Microwave Theory Tech.*, vol. 47, pp. 1070–1076, July 1999.

[3] N.-S. Cheng, P. Jia, D. B. Rensch, and R. A. York, "A 120-W X-band spatially combined solid-state amplifier," *IEEE Trans. Microwave Theory Tech.*, vol. 47, pp. 2557–2561, Dec. 1999.

[4] P. Jia, L.-Y. Chen, A. Alexanian, and R. A. York, "Multioctave spatial power combining in oversized coaxial waveguide," *IEEE Trans. Microwave Theory Tech.*, vol. 50, pp. 1355–1360, May 2002.

[5] P. Jia and R. A. York, "A compact coaxial waveguide combiner design for broadband power amplifiers," in *IEEE MTT-S Int. Microwave Symp. Dig.*, vol. 1, Pheonix, AZ, May 2001, pp. 43–46.

[6] P. Jia, L.-Y. Chen, A. Alexanian, and R. A. York, "Broadband high power amplifier using spatial power combining technique," in *IEEE MTT-S Int. Microwave Symp. Dig.*, vol. 3, 2003, pp. 1871–1874.

[7] D. B. Rutledge *et al.*, "Failures in power-combining arrays," *IEEE Trans. Microwave Theory Tech.*, vol. 47, pp. 1077–1082, July 1999.

[8] E. R. Brown and J. F. Harvey, "System characteristics of quasioptical power amplifiers," *IEEE Circuits Syst. Mag.*, vol. 1, pp. 22–36, Apr. 2001.

[9] R. A. York, "Some considerations for optimal efficiency and low noise in power combiners," *IEEE Trans. Microwave Theory Tech.*, vol. 49, pp. 1477–1482, Aug. 2001.

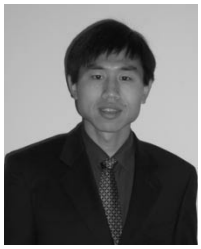

Pengcheng Jia (S'98–M'03) received the B.S. degree in electronics science and information system from Nankai University, Tianjin, China, in 1995, the M.S. degree in electronic engineering from Tsinghua University, Beijing, China, in 1998, and the Ph.D. degree in electrical and computer engineering from the University of California at Santa Barbara (UCSB), in 2002. His doctoral research at UCSB involved the development of waveguide-based broad-band high-power spatial power combiners.

He is currently with CAP Wireless Inc., Newbury Park, CA.

Lee-Yin Chen (S'98) received the B.S. degree in electrical engineering from the National Taiwan University, Taipei, Taiwan, R.O.C., in 1997, and the M.S. and Ph.D. degrees in electrical engineering from the University of California at Santa Barbara (UCSB), in 1999 and 2003, respectively. Her doctoral research at UCSB involved the development of power-amplifier and spatial power-combining systems at Ka-band.

She is currently with Agile Materials and Technologies, Goleta, CA.

Angelos Alexanian (S'92–M'93) received the B.S. degree (*summa cum laude*) from the Virginia Polytechnic Institute and State University, Blacksburg, in 1991, the M.S. degree from The University of Michigan at Ann Arbor, in 1993, and the Ph.D. degree from the University of California at Santa Barbara in 1997, all in electrical engineering. His doctoral dissertation concerned electromagnetic (EM) analysis of periodic structures using the finite-difference time-domain technique and development of broad-band spatial power-combining schemes.

From 1997 until 1999, he was with the M/A-COM Corporate Research and Development Group. He then joined the RFMD Boston Design Center, where he designed RF integrated circuits (RFICs) for the digital cellular product line. Since October 2000, he has been with Narad Networks, Westford, MA, where he is responsible for the design and development of an RFIC transceiver chipset employed for 100-MB/s–1-Gb/s digital links over a cable-television infrastructure.

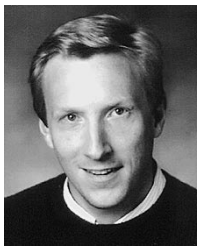

Robert A. York (S'85–M'89–SM'99) received the B.S. degree in electrical engineering from the University of New Hampshire, Durham, in 1987, and the M.S. and Ph.D. degrees in electrical engineering from Cornell University, Ithaca, NY, in 1989 and 1991, respectively.

He is currently a Professor of electrical and computer engineering at the University of California at Santa Barbara (UCSB), where his group is currently involved with the design and fabrication of novel microwave and millimeter-wave circuits, high-power microwave and millimeter-wave amplifiers using spatial combining and wide-bandgap semiconductor devices, and application of ferroelectric materials to microwave and millimeter-wave circuits and systems.

Dr. York was the recipient of the 1993 Army Research Office Young Investigator Award and the 1996 Office of Naval Research Young Investigator Award.